Numerical Modelling of a Flyer Plate Electromagnetic Accelerator

Bucur M. Novac, *Senior Member, IEEE*, Kaashif Omar, Neal Graneau, Ivor R. Smith, *Senior Member, IEEE*, and Mark Sinclair, *Member, IEEE*

***Abstract*—A joint program involving the study and practical performance of a foil-flyer electromagnetic accelerator has recently been initiated by Atomic Weapons Establishment, Aldermaston, and Loughborough University. As an initial phase of the work, both 0-D and 2-D numerical models for the foil-flyer accelerator have been developed. The 0-D model, although very crude, is capable of providing an insight into the accelerator phenomena and is currently used for parametric design studies. The 2-D model is based on the well-proven Loughborough filamentary modeling technique and is capable of accurately calculating the 2-D distribution of current, velocity, acceleration, and temperature of the flyer, together with the complete distribution of the magnetic and electric fields generated during a shot. The paper presents the two models and compares typical theoretical predictions with the corresponding experimental results.**

***Index Terms*—Electromagnetic accelerators, electromagnetism, filamentary modeling, pulsed power.**

I. Introduction

A NUMBER of research programs have been recently carried out which exploit the electromagnetic forces generated by the current flowing in a strip-line conductor geometry [1]–[5]. These experiments have been developed to conduct isentropic compression experiments (ICE) as well as small-scale flyer plate impact shock-wave tests. The present paper however is dedicated to a capacitor-based high current pulsed power system designed and developed at Atomic Weapons Establishment (AWE) to simulate the mechanical impulse imparted to a target by the exo-atmospheric deposition of cold X-rays. The impulse is generated when a thin layer of the target material is ablated outwards, and at the same time, an inwardly directed shockwave is generated to conserve momentum; this travels to the back surface of the target and can cause mechanical damage including spalling or delamination. The effect of the shockwave is of importance and a method to recreate it without the need for X-rays has been developed. In order to achieve a reliable and accurate simulation of this effect in a planar target, it is necessary to create a planar shockwave which can travel through the material.

Manuscript received November 29, 2011; revised January 20, 2012; accepted February 9, 2012. Date of publication April 5, 2012; date of current version October 5, 2012.

B. M. Novac and I. R. Smith are with the School of Electronic, Electrical and Systems Engineering, Loughborough University, Leicestershire, LE11 3TU, U.K. (e-mail: B.M.Novac@lboro.ac.uk; i.r.smith@lboro.ac.uk).

K. Omar, N. Graneau, and M. Sinclair are with the Hydrodynamics Department, AWE, Aldermaston, Reading, RG7 4PR, U.K. (e-mail: Kaashif.Omar@awe.co.uk; Neal.Graneau@awe.co.uk; mark.sinclair@awe.co.uk).

Color versions of one or more of the figures in this paper are available online at http://ieeexplore.ieee.org.

Digital Object Identifier 10.1109/TPS.2012.2189236

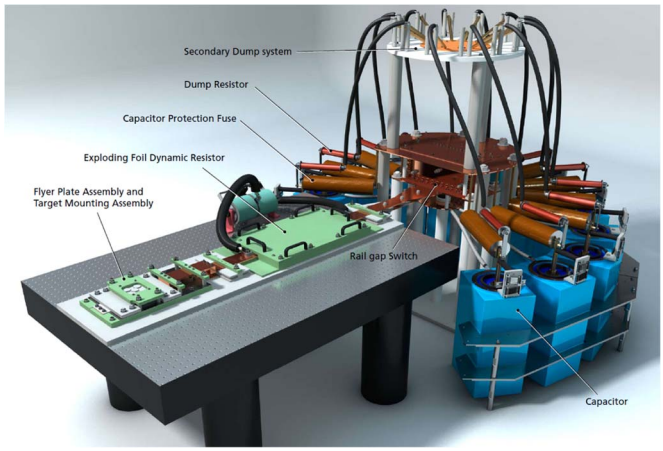

Fig. 1. AMPERE facility for accelerating flyer plates installed at AWE Aldermaston.

The system developed at AWE is based on a series RLC circuit which has a time varying resistance and inductance due to both an exploding metallic fuse and the dynamics of a flyer. A shot consists of charging the capacitor, with the circuit open, followed by discharging it using a triggerable closing switch. The system termed AMPERE (Fig. 1) is fully described in [6], but for clarity the electromagnetic accelerator, part of a parallel-plate transmission line (historically termed a "strip" line), is presented in Fig. 2. The electromagnetic accelerator has a simple configuration, consisting of three parts:

- a relatively thick and immovable metallic part, termed the "stator," that is mounted on top of a heavy support (a table, shown in Fig. 1);
- a thin dielectric layer, mounted above the stator, which can withstand the electric field developed between the flyer and the stator during a shot; its thickness determines the initial (vertical) distance between the two components which is of paramount importance for the flyer dynamics;
- a thin metallic foil, termed the "flyer," which is the moving part and is mounted on top of the dielectric layer.

The flyer and the stator are electrically connected to the transmission line, with the same current flowing in opposite directions through the two components and generating magnetic fields and repulsive forces. All accelerator parts are manufactured to be as flat as possible to avoid any trapped air between the parallel mounted components.

In what follows all the components are considered as *incompressible bodies*, with both 0-D and 2-D models neglecting their

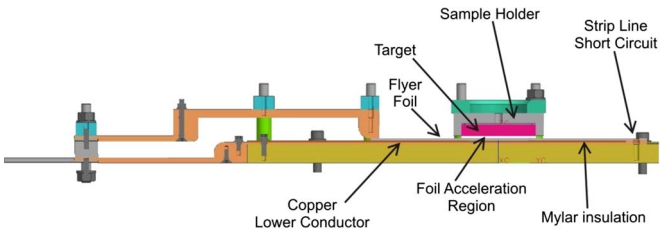

Fig. 2. Electromagnetic accelerator embedded in the parallel-plate transmission line (strip line) of the AMPERE pulsed power system.

elastoplastic properties, together with the associated production of shock waves. Naturally following from this, the variation of the electrical conductivity of metals due to pressure is also neglected.

II. 0-D Model

A. Generalities

The 0-D model is based on the *main* simplifying assumption that the current flows homogeneously, through both the flyer and the stator. This assumption has a series of consequences:

- the flyer is accelerated without changing its shape, i.e., it remains flat at all times during a shot, and therefore only one velocity has to be calculated;
- the Joule energy is uniformly deposited within the two metallic components, i.e., during an experiment, there is only one (bulk) temperature for the flyer and another one for the stator.

B. Circuit Equations

The equivalent circuit for the system is shown in Fig. 3 and can be described by the two first-order differential equations:

$$V_0 - \frac{Q(t)}{C} = \left[R_\mathrm{b} + R_\mathrm{fuse}(W_\mathrm{fuse}) + R_\mathrm{flyer}(W_\mathrm{flyer}) + \frac{dL_\mathrm{acc}}{dt}\right] I(t) + \left[L_\mathrm{b} + L_\mathrm{acc}(t)\right] \frac{dI}{dt} \quad (1)$$

$$I(t) = \frac{dQ}{dt} \quad (2)$$

where C is the bank capacitance initially charged to a voltage V_0. I(t) and Q(t) are the circuit current and the corresponding charge injected into the circuit at time t, R_b and L_b are the total circuit resistance and self-inductance, excepting the fuse and flyer resistances (R_fuse and R_flyer) and the accelerator self-inductance L_acc, a time-dependent variable. For simplicity, both R_b and L_b are regarded as time invariant during a shot.

The Loughborough exploding metallic fuse model (Fig. 4), provides the variation of its initial resistivity (and therefore its resistance) during the explosion. It requires calculation of the specific Joule energy W_fuse deposited during the shot, which is obtained by integration of the following differential equation:

$$\frac{dW_\mathrm{fuse}}{dt} = \frac{I(t)^2 R_\mathrm{fuse}}{\mathrm{mass}_\mathrm{fuse}} \quad (3)$$

where $\mathrm{mass}_\mathrm{fuse}$ is the fuse mass and the fuse resistance is a function of deposited energy, i.e., $R_\mathrm{fuse} = R_\mathrm{fuse}(W_\mathrm{fuse})$.

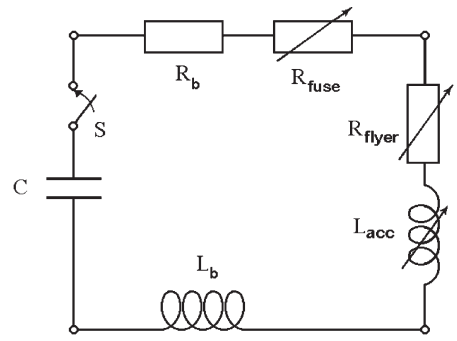

Fig. 3. Equivalent electrical circuit of the AMPERE pulsed power system.

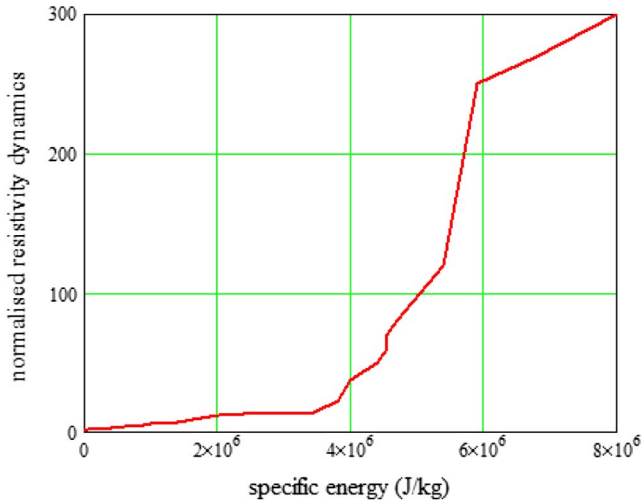

Fig. 4. Phenomenological model for exploding fuse, the normalized variation of resistivity during an explosion is shown in the vertical scale as a number that indicates how many times the initial value has increased for a specific Joule energy deposited into the fuse.

A similar equation (i.e., the same model) is used firstly to calculate the Joule energy deposited into the flyer (W_flyer) and then to estimate its resistance (R_flyer).

The *initial* self-inductance of the accelerator is that of a parallel plate transmission line ("strip line") of length l, width w, and plate separation d, for which the following simple formula exists:

$$L_\mathrm{line} = \mu_0 \frac{dl}{w} K\left(\frac{d}{w}\right). \quad (4)$$

Although the transmission line has a very simple geometry, the best estimate for the correction factor K (dependent on the ratio between the separation distance d between the plates over the plate width w) is given in literature only in the form of a figure [7]. However, by using experimental results for parallel plate capacitors (sic!) [8], an analytical form for the correction factor can be derived, allowing the following accurate formula for the accelerator self-inductance during acceleration to be obtained:

$$L_\mathrm{acc}(y) = \begin{cases} \frac{\mu_0 l}{\pi} \ln\left(\frac{8y^2+w^2}{2wy}\right) & \text{for } y > 2w \\ \mu_0 l \frac{1}{\frac{w}{y}+1.21-0.11\frac{y}{w}+\left(1-\frac{y}{2w}\right)^6} & \text{otherwise} \end{cases} \quad (5)$$

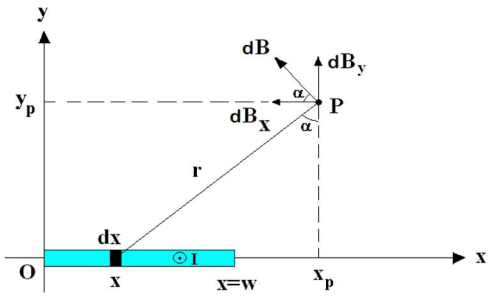

Fig. 5. Calculation of the magnetic field produced by the stator at a point $P(x_\mathrm{p}, y_\mathrm{p})$ with current flowing along the Oz-axis; an elementary straight conductor is highlighted, situated at a distance x from origin, having a width dx, carrying a surface current density $J = I/w$ and producing an elementary magnetic field dB at the point P.

where y(t) is the time-varying flyer position, with $y(t = 0) = d$ being the initial distance between stator and flyer. The time rate of change of the accelerator self-inductance can be easily calculated at all times as

$$\frac{\partial L_\mathrm{acc}}{\partial t} = \frac{\partial L_\mathrm{acc}}{\partial y}\frac{\partial y}{\partial t} = v_\mathrm{y}(t)\frac{\partial L_\mathrm{acc}}{\partial y} \tag{6}$$

where $v_\mathrm{y}(t)$ is the time-dependent flyer velocity.

C. Flyer Dynamics

For calculating forces, the 0-D model considers both *the stator and the flyer as infinitely thin plates*, made from a large collection of straight elementary conductors (parallel to Oz) carrying the *same* surface current density $J = I/w$ (see Fig. 5), over their width dx. The magnetic field produced at a point $P(x_\mathrm{p}, y_\mathrm{p})$ by an elementary conductor situated a distance x from the origin (Fig. 5) is $dB = (\mu_0 J/2\pi r)dx$, where $r = \sqrt{(x_p - x)^2 + y_p^2}$.

By integrating the magnetic fields produced by all elementary conductors, the components of the total magnetic flux density produced at P by the stator are given by

$$B_x(x_p, y_p) = -\frac{\mu_0 y_p J}{2\pi}\int_0^w \frac{dx}{(x_p - x)^2 + y_p^2} = \frac{\mu_0 I}{2\pi w}\left[\tan^{-1}\left(\frac{x_p - w}{y_p}\right) - \tan^{-1}\left(\frac{x_p}{y_p}\right)\right] \tag{7}$$

$$B_y(x_p, y_p) = \frac{\mu_0 J}{2\pi}\int_0^w \frac{(x_p - x)dx}{(x_p - x)^2 + y_p^2} = \frac{\mu_0 I}{4\pi w} ln\left[\frac{x_p^2 + y_p^2}{y_p^2 + (x_p - w)^2}\right]. \tag{8}$$

Interaction of the magnetic field generated by the stator with the current $Jdx = Idx/w$ flowing through an elementary

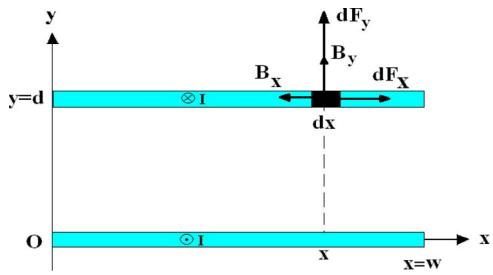

Fig. 6. Calculation of the differential force acting on a flyer elementary conductor.

conductor of width dx and length l of the flyer produces a differential force having two components

$$dF = \frac{Idx}{w}(\boldsymbol{l}\times\boldsymbol{B}) = \frac{Idx}{w}\begin{vmatrix} \boldsymbol{k_x} & \boldsymbol{k_y} & \boldsymbol{k_z} \\ 0 & 0 & -l \\ B_x & B_y & 0 \end{vmatrix} = \frac{Ildx}{w}(B_y\boldsymbol{k_x} - B_x\boldsymbol{k_y}).$$

The first of these is perpendicular to the flyer surface (dF_y in Fig. 6)

$$dF_y\Big|_{y=d} = -\frac{Il}{w}B_x(x,d)\,dx = -\frac{\mu_0 I^2 l}{2\pi w^2}\left[\tan^{-1}\left(\frac{x-w}{d}\right) - \tan^{-1}\left(\frac{x}{d}\right)\right]dx \tag{9}$$

and is responsible for the vertical acceleration of the flyer. The other is parallel to the flyer surface (dF_x in Fig. 6) and is attempting to change its shape. The action of this force is not present in what follows, since the elastoplasticity of the flyer is neglected and the total accelerating force F_y, acting on the flyer when a distance $y = d$ from the stator, is found by integration as

$$F_y(d) = \int_0^w dF_y = \frac{\mu_0 I^2 l}{2\pi w^2}\left[2w\tan^{-1}\left(\frac{w}{d}\right) - dln\left(\frac{d^2 + w^2}{d^2}\right)\right]. \tag{10a}$$

This is a more accurate calculation of the accelerating force than simply estimating it from the resultant magnetic pressure produced by both the stator and the flyer

$$F_y = \frac{(2B)^2}{2\mu_0}lw = \frac{\left(2\mu_0\frac{I}{2w}\right)^2}{2\mu_0}lw = \mu_0\frac{I^2 l}{2w} \tag{10b}$$

as used in similar published 0-D modelling [9]. It is clear that (10b), calculated using the magnetic flux density B produced on the stator (or flyer) surface, provides a force that remains constant during acceleration and is always larger than the force calculated using (10a).

Apart from the electromagnetically produced force, the flyer dynamics is influenced by (at least) three forces, all opposing its initial phase of acceleration.

The first of these is caused by friction with the ambient gas (air in the present experiments), with the drag force expressed as

$$F_\mathrm{drag}(v) = \frac{1}{2}\rho_\mathrm{gas}v^2 C_\mathrm{drag} lw \tag{11}$$

TABLE I
FITTING COEFFICIENTS USED IN (13)

Coefficient	Phase	
	i = 1	i = 2
$K_i^{\text{flyer-target}}$	1	0.63
$K_i^{\text{flyer-stator}}$	0	1

where ρ_{gas} is the gas density and v is the flyer velocity. The drag coefficient for a plate is approximated as $C_{\text{drag}} \approx 1.28$. As will be evident later, due to the low values of the flyer velocity, this force is negligible in the present experimentation.

The second is simply the constant gravitational force

$$G = m_{\text{flyer}} g \tag{12}$$

where m_{flyer} is the flyer mass and g is the gravitational constant.

The third force appears whenever a solid target plate is initially mounted a distance $d_{\max}$ above and parallel to the flyer. The target introduces extremely complex interaction phenomena, for which a simplified model is presented below. During a shot, two phases in the flyer dynamics can be distinguished in the flyer dynamics, due to the effect of the target. These are both related to the compression and decompression of two gas volumes: the first located between the flyer and the target and second between the flyer and the plastic insulator covering the stator, with the flyer playing the role of a piston. During the first phase, the pressure build-up eventually produces shock waves, and their complex interactions with the target and flyer eventually reverse the direction of the flyer velocity, which is the second phase. Since the careful construction of the initial setup eliminates initial air pockets between the flyer and the insulator covering the stator, it can be assumed that there is initially a vacuum formed behind the accelerating flyer (a phenomenon used in the development of the technology for reliable multi-MA transmission lines [10]), but this volume is later filled with gas. The second phase of acceleration is much more complicated to model as it involves not only the decompression of the gas, but also the elastic and plastic properties and thicknesses of both the flyer and target. For simplicity, only adiabatic compression processes are assumed as suggested in [11], and therefore the retarding force on the flyer can be estimated as

$$F_{\text{flyer-target}}(y) = p_0 l w \left(\frac{d_{\max}}{d_{\max} + d - y} K_{\text{i}}^{\text{flyer-target}} \right)^{\gamma} \tag{13a}$$

corresponding to the volume of gas compressed between the flyer and target and

$$F_{\text{flyer-stator}}(y) = p_0 l w \left(\frac{d_{\max}}{y - d} K_{\text{i}}^{\text{flyer-stator}} \right)^{\gamma} \tag{13b}$$

corresponding to the gas compressed between the flyer and the plastic covering the stator; p_0 is the ambient gas pressure, the adiabatic factor is approximated as $\gamma \approx 7/5$ and the coefficients K_i $(i = 1, 2)$ given in Table I are determined such that the theoretical calculations match the experimental data.

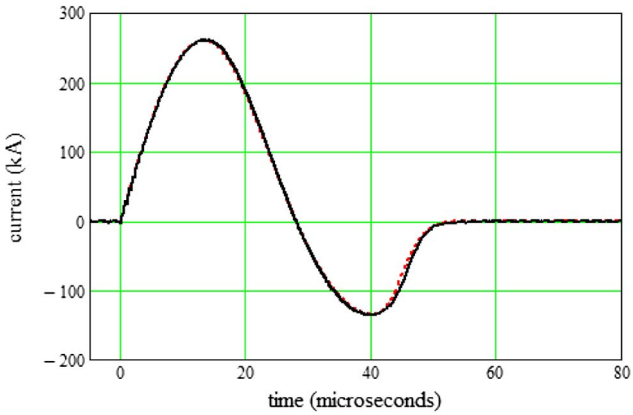

Fig. 7. System current during a shot, continuous line: experiment; dotted line: 0D model.

Taking into account all forces, the differential equations of motion can be written as

$$\frac{dv}{dt} = \frac{1}{m_{\text{flyer}}} \left(F_{\text{y}} + (-1)^{\text{i}} F_{\text{drag}} - G - F_{\text{flyer-target}} + F_{\text{flyer-stator}} \right) \tag{14}$$

$$\frac{dy}{dt} = v \tag{15}$$

The flyer begins to move from its initial position only when $F_y > G + \text{F}_{\text{flyer-target}}(y = d)$.

D. Theoretical Calculations Compared to Experimental Data

By integrating the system of first-order differential equations (1)–(3), (14), and (15), using for example the MATHCAD 15 Runge-Kutta built-in subroutine, the solution can be easily found.

In the example below, the main AMPERE parameters [6] are: $C = 129$ μF, $V_0 = 21.5$ kV, $R_b = 8.8$ mΩ, and $L_b = 650$ nH. The exploding fuse is made from 50 μm thick aluminium foil, 85 mm wide and 300 mm long. The stator is made from 1 mm thick copper sheet, 90 mm wide and 300 mm long, and the flyer is made from 300 μm thick aluminium foil, 90 mm wide and 300 mm long. A complete run over 120 μs under Windows 7 on a laptop with an Intel Core i7 CPU @ 2.67 GHz with 4 GB RAM takes just 2 seconds.

Figs. 7–11 show the wealth of information provided by the theoretical calculations and compares these with corresponding experimental data.

Analysis of calculations made with the 0-D model shows that although the model is very crude, it can nevertheless be used to provide a basic understanding of the phenomena involved. It can also prove very useful in minimizing the calculation time when detailed parameter studies are conducted during the tedious design procedure for a novel accelerator.

III. 2-D MODEL

A. Generalities

The 2-D model is based on the well-proven Loughborough filamentary modelling, which has been in use for many years.

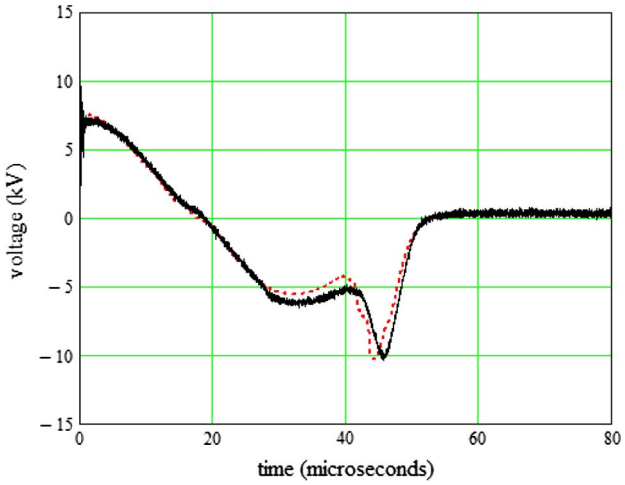

Fig. 8. Voltage across AMPERE transmission line, incorporating the exploding metallic fuse and the electromagnetic accelerator, continuous line: experiment; dotted line: 0D model.

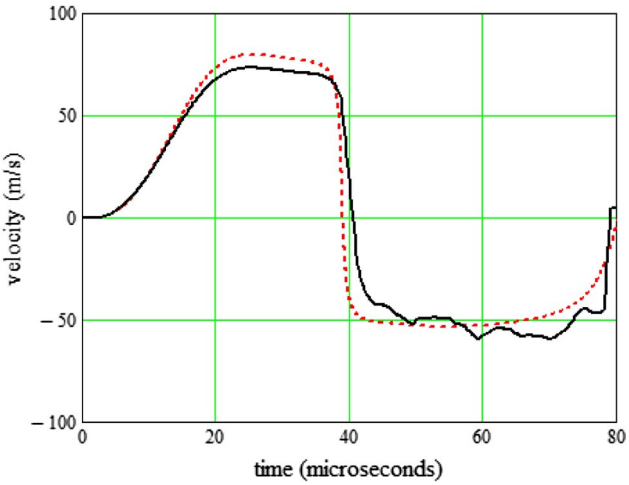

Fig. 9. Time dependence of the flyer velocity; two phases of acceleration are present, defined by the sign of velocity and corresponding to the following time intervals (in μs): 0–40 (positive), 40–80 (negative), continuous line: experimental data from heterodyne velocimetry technique [1] dotted line: 0D model.

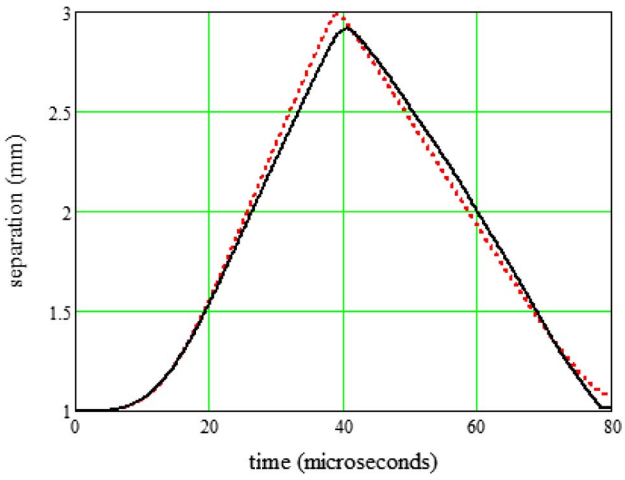

Fig. 10. Flyer dynamics inside the space between the insulation covering the stator and the target; the initial axial separation between the flyer and the stator is 1 mm with a target mounted at 2 mm above the flyer continuous line: integrated experimental data of Fig. 7; dotted line: 0D model.

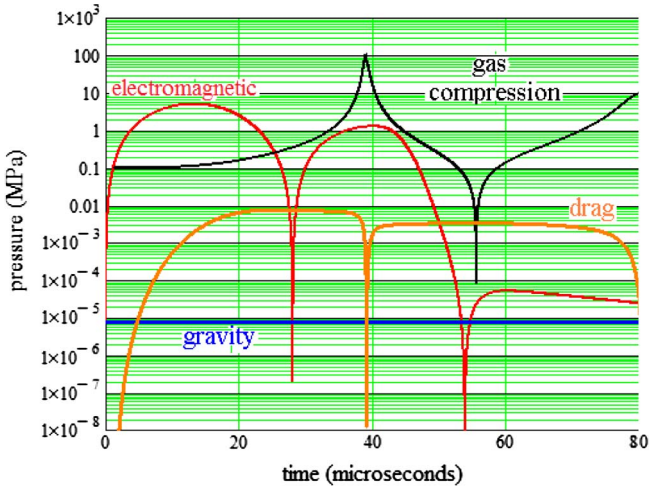

Fig. 11. Theoretical predictions of the various pressures acting on the flyer during the different acceleration phases; note the logarithmic scale.

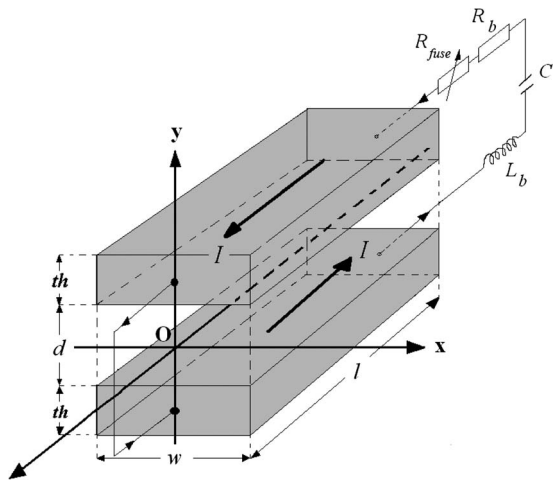

Fig. 12. Parallel-plate electromagnetic accelerator, (for simplicity, the stator and flyer are shown identical).

A number of original features have recently been introduced into the standard approach (also termed network mesh or mesh-matrix method), mostly related to the fast dynamics of imploding/exploding metallic structures. The technique has been successfully applied by Loughborough along the years in a very wide range of pulsed power applications, including pulsed ultrahigh magnetic field coils [12], explosively driven flux-compression generators [13], [14], single and multiturn electromagnetic launchers [15]–[17], electromagnetic launchers [15]–[17], electromagnetic compression [18], and the design of various types of high-voltage air core pulsed transformers [19].

The starting point in applying the technique to the present task is to define Cartesian (rectangular) coordinates, with the transmission line and therefore its current I along and positioned symmetrically about the Oz axis, and with the short-circuited end in the Oxy plane as shown in Fig. 12. The method is based on two *fundamental hypotheses*:

I) the current *direction* inside the metallic components is known *a priori*, i.e., it flows only along the Oz axis;

II) the current density is uniformly distributed inside each filament.

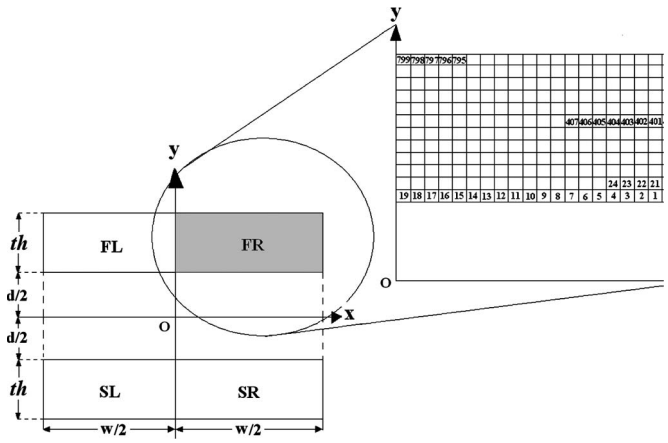

Fig. 13. Filamentary representation of the electromagnetic accelerator. By symmetry, only currents in one half have to be calculated, and, for simplicity, the stator and flyer are shown as identical.

Implementation of the method requires:

I) the conductors to be "cut" or "divided" into parallel, isolated filaments along the Oz axis (the best way is to visualize the filamentary representation as conductors comprising a large number of much thinner conductors each coated with an infinitely thin insulating layer), such that the filamentary currents flow uniquely along this direction (Fig. 13). The cross section of the individual filaments, clearly related to their total number N, must be sufficiently small for the uniform current density hypothesis to be valid.

II) the filaments form an electric circuit network for which Kirchhoff-type equations can be written. The resulting system of N algebraic equations is firstly solved for the "i-dots" (i.e., the time rate of change of the filamentary currents), and the resulting first-order differential equations are time integrated using the initial conditions and (for example) a Runge-Kutta subroutine. The results, in the form of filamentary time-dependent currents, provide a wealth of information on the system, as shown later.

By inspection, symmetry allows both of the two conductors forming the accelerator (i.e., the flyer F and the stator S) to be represented by two segments (i.e., left side FL and right side FR), through which the same current flows as shown in Fig. 13. The technique therefore requires only calculation of the filamentary currents flowing through *only one segment* of each conductor, which enables the total number of filamentary currents flowing to be doubled.

B. Filamentary Kirchhoff Equations

Consider the current in FR, representing half of the total current I, decomposed into N *identical* parallel rectangular filamentary currents. Each of these is homogeneously distributed inside the rectangular cross-section area with width $\Delta xf = w/2n_{\mathrm{x}}$ and height $\Delta yf = th/n_{\mathrm{y}}$, where w and th are the flyer width and thickness and n_{y} and n_{x} represent integers with $N = n_{\mathrm{y}}n_{\mathrm{x}}$. Numbering of the filamentary currents begins at the lower right-hand side of FR, as in Fig. 13, to allow easy implementation of the symmetry. The coordinates of the center of the i-th filament are

$$xf_{\mathrm{i}} = \frac{w}{2} - \left(\mathrm{mod}(i, n_{\mathrm{x}}) + \frac{1}{2}\right)\Delta xf \tag{16}$$

$$yf_{\mathrm{i}} = \frac{d}{2} + \left(\mathrm{floor}\left(\frac{i}{n_{\mathrm{x}}}\right) + \frac{1}{2}\right)\Delta yf \tag{17}$$

where $\mathrm{mod}(i,n)$ and $floor(x)$ are subroutines returning the remainder of i when divided by n and the greatest integer $\leq$ x, respectively. An identical procedure is applied to find the coordinates of the centers of the stator filaments. For reasons related to limiting the computational time, it was decided to divide the stator plate into the same number of filaments as the flyer plate. It is important to note however that although the currents flowing through the stator filaments are precisely those flowing through the flyer filaments, the model allows the stator filaments to have a different geometry. However, for simplicity, both Figs. 12 and 13 show an accelerator with the flyer and the stator being identical plates, but in many cases, the stator plate is much thicker than the flyer plate and does not necessarily have the same width. In such cases, the filamentary cross-section sides for the rectangular stator filaments are larger than that for the filaments in the flyer, i.e., $\Delta xs > \Delta xf$; $\Delta ys > \Delta yf$.

By applying Kirchhoff's current and voltage laws, the total current I is obtained in terms of the filamentary currents I_{i} as

$$I = 2\sum_{\mathrm{i}=0}^{\mathrm{N}-1} I_{\mathrm{i}} \tag{18}$$

and the N first-order differential voltage equations for the filamentary currents $(i = 0 \ldots N-1)$ as:

$$\begin{aligned} V_0 - \frac{Q}{C} - 2\left[R_b + R_{\mathrm{fuse}}(W_{\mathrm{fuse}})\right]\sum_{j=0}^{N-1} I_j - \left[(R_f)_i + (R_s)_i\right] I_i \\ - \sum_{j=0}^{N-1} \big[\mathrm{DMFRFR}_{i,j} + \mathrm{DMFRFL}_{i,j} - \mathrm{DMFRSR}_{i,j} \\ - \mathrm{DMFRSL}_{i,j} - \mathrm{DMSRFR}_{i,j}(1-\delta_{i,j}) \\ - \mathrm{DMSRFL}_{i,j}\big] I_j \\ = \sum_{j=0}^{N-1} \big[\mathrm{MFRFR}_{i,j} + \mathrm{MFRFL}_{i,j} + \mathrm{MSRSR}_{i,j} \\ + \mathrm{MSRSL}_{i,j} - \mathrm{MFRSR}_{i,j} - \mathrm{MFRSL}_{i,j} \\ - \mathrm{MSRFR}_{i,j}(1-\delta_{i,j}) - \mathrm{MSRFL}_{i,j} \\ + 2L_b\big]\left(\frac{dI}{dt}\right)_j \end{aligned} \tag{19}$$

with the time rate of change of the charge injected into the circuit

$$\frac{dQ}{dt} = 2\sum_{\mathrm{i}=0}^{\mathrm{N}-1} I_{\mathrm{i}} \tag{20}$$

where $\delta_{\mathrm{i,j}}$ is the Kronecker delta function (i.e., $\delta_{\mathrm{i,j}} = 1$ if $i = j$ and $\delta_{\mathrm{i,j}} = 0$ if $i \neq j$). The resistance $(R_{\mathrm{f}})_{\mathrm{i}}$ of the i-th flyer filament depends on its temperature, i.e., on the specific Joule energy $(W_{\mathrm{f}})_{\mathrm{i}}$ deposited into the filament during the shot

$$(R_{\mathrm{f}})_{\mathrm{i}} = \frac{l}{\sigma\left((W_{\mathrm{f}})_{\mathrm{i}}\right)\Delta yf\Delta xf} \tag{21}$$

where σ is the temperature-dependent electrical conductivity of the flyer material and the time rate of change of the Joule energy is

$$\left(\frac{dW_{\rm f}}{dt}\right)_{\rm i} = \frac{I_{\rm i}^2 (R_{\rm f})_{\rm i}}{{\rm mass}_{\rm f}} \tag{22}$$

where the filamentary mass is simply ${\rm mass}_{\rm f} = {\rm mass}_{\rm flyer}/2N$. Similar equations apply for the stator filaments.

In (19) $\rm MFRFR_{i,j}$ represents the mutual inductance between filaments i and j, both situated in the right-hand side of the flyer, while $\rm MFRSL_{i,j}$ is for the mutual inductance of a pair of filaments situated in the flyer right-hand side and stator left-hand side, etc. The time rate of change of the mutual inductance between a pair of filaments i and j is written as $\rm DMFRFR_{i,j}$, when the filaments are both situated in the flyer right-hand side, and so on. Because the stator shape remains unchanged, $\rm DMSRSR_{i,j} = DMSRSL_{i,j} = 0$ for any i and j. Note also that MSRFR and DMSRFR are the transpose of MFRSR and DMFRSR.

C. Mutual Inductance of Two Rectangular Filaments

Implementation of simple formulae for the filamentary self- and mutual inductances seems straightforward and using such a technique [20] reported the successful modelling of transmission lines with parallel-plate geometry. Due to the simplicity of their model, i.e., no Joule effects or forces were taken into account, the authors were able to use a very large number of filaments having a square cross section. When the same technique was applied to the flyer plate accelerator, it failed, i.e., the inverse of the inductance matrix could not be calculated numerically. An analysis showed that *because of their rather low number*, and because of the particular geometry of the flyer (i.e., a thin and rather wide plate), the filaments have a particular rectangular cross section with *one side many tens of times larger than the other* (like a very thin plate), and in such a case, the simple technique used in [20] for calculating inductances is obviously invalid.

An *exact* formula is available [21] for calculating the mutual inductance M between two parallel filaments i and j

$$M_{\rm i,j} = \frac{\mu_0 l}{2\pi}\left(\ln\frac{l+\sqrt{l^2+{\rm dist}_{\rm i,j}^2}}{{\rm dist}_{\rm i,j}} - \frac{\sqrt{l^2+{\rm dist}_{\rm i,j}^2}}{l} + \frac{{\rm dist}_{\rm i,j}}{l}\right) \tag{24}$$

where $\rm dist_{i,j}$ is the geometrical mean distance (GMD) between the two filaments and not simply the distance between their cross-section centers as in [20]. The problem is that although the GMDs of rectangular areas were calculated at the beginning of the XXth century (see for example [22]), the published results are restricted only to symmetrically positioned rectangles. Fortunately, Tasker has recently solved this complicated issue and obtained the analytical formulae for GMDs between two asymmetrically positioned parallel filaments having rectangular cross sections. His work was related to modelling electromagnetically driven ICE using parallel plate geometry, and the filamentary technique was used to provide the initial current distribution to be used as initial data for complex magnetohydrodynamic codes, such as ALEGRA [23]. The formulae to calculate GMDs presented below are taken from his work [24], [25] and use the same notation and sign convention as used in [22], [24], [25]: the origin is taken as the left-hand side of the lower rectangle, $-\alpha$ represents the distance to the left, and β to the right-hand side of the upper rectangle, and p is the distance between the two rectangles. If the upper rectangle has a width c and the lower has a width a, the distance between the perpendiculars through their centers is $0.5(\beta-\alpha-a)$.

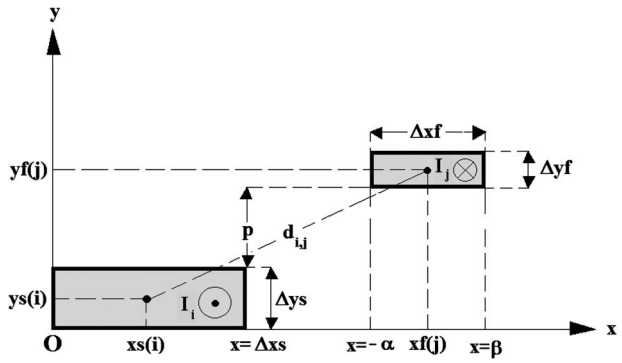

Fig. 14. Rectangular cross sections of two asymmetrically positioned parallel filaments. Filament i is in the right-hand side of the stator (SR) and filament j is in the same side of the flyer (FR), with the currents in the two filaments flowing in different directions. The parameters used in calculating the GMD are shown as p, α and β. The distance $d_{\rm i,j}$ between their centers is also shown.

As an example, the GMD of the two parallel filaments with rectangular cross section defined in Fig. 14 is

$${\rm dist}_{\rm i,j} = \exp(G) \tag{25}$$

where the function G is obtained from

$$\begin{aligned} G(\Delta xf,\Delta yf,\Delta xs,\Delta ys,p,\alpha,\beta) &= -\frac{3}{2} + \frac{1}{\Delta xf\cdot\Delta yf\cdot\Delta xs\cdot\Delta ys} \\ &\times[f(\beta-\Delta xf,p+\Delta yf+\Delta ys) - f(\beta-\Delta xf,p+\Delta yf) \\ &- f(\beta,p+\Delta yf+\Delta ys) + f(\beta,p+\Delta yf) \\ &- f(\alpha+\Delta xf,p+\Delta yf+\Delta ys) + f(\alpha+\Delta xf,p+\Delta yf) \\ &+ f(\alpha,p+\Delta yf+\Delta ys) - f(\alpha,p+\Delta yf) \\ &- f(\beta-\Delta xf,p+\Delta ys) + f(\beta-\Delta xf,p) \\ &+ f(\beta,p+\Delta ys) - f(\beta,p) + f(\alpha+\Delta xf,p+\Delta ys) \\ &- f(\alpha+\Delta xf,p) - f(\alpha,p+\Delta ys) + f(\alpha,p)] \end{aligned} \tag{26}$$

with

$$p = |ys(i) - yf(j)| - \frac{\Delta ys+\Delta yf}{2}$$

$$\alpha = -|xs(i) - xf(j)| + \frac{\Delta xf-\Delta xs}{2}$$

$$\beta = |xs(i) - xf(j)| + \frac{\Delta xs+\Delta xf}{2}$$

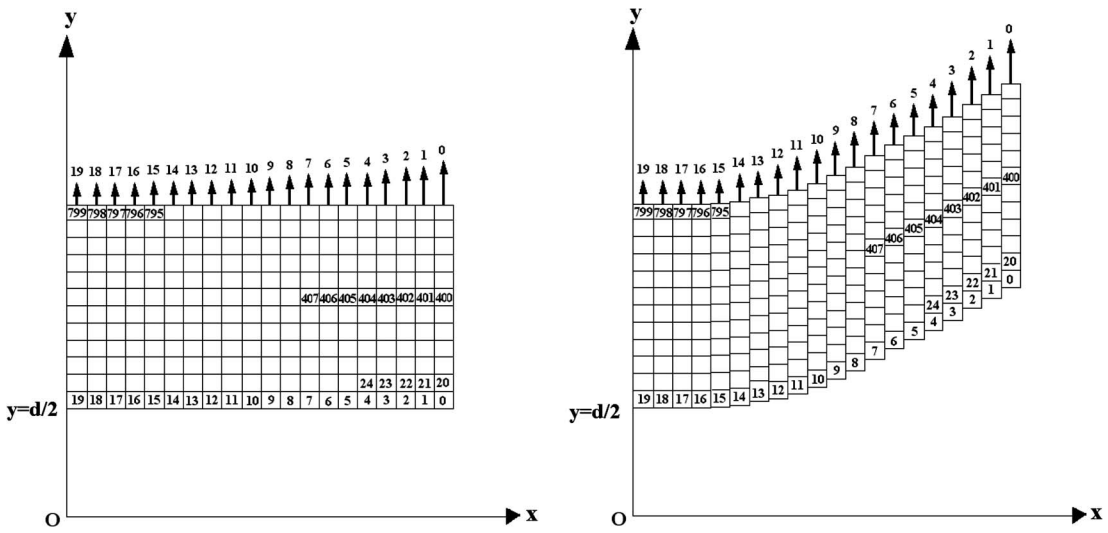

Fig. 15. (Left) Forces acting on filamentary columns at $t = 0$, shown as arrows and numbered from right to left, (Right) Filamentary representation of 2D conductor dynamics during the first moments of a shot.

and where the function f is given by

$$f(\gamma,\omega) = \gamma^2(\gamma^2 - 6\omega^2)\left(\frac{1}{48}\ln(\gamma^2+\omega^2) - \frac{7}{288}\right) + \frac{\omega^4}{48}\ln(\gamma^2+\omega^2) - \frac{\gamma\omega}{6}(\omega^2 \cdot f1 + \gamma^2 \cdot f2) \quad (27)$$

with

$$f1 = \begin{cases} \frac{\pi}{2} & \text{if } \omega = 0 \\ \tan^{-1}\left(\frac{\gamma}{\omega}\right) & \text{otherwise} \end{cases} \quad f2 = \begin{cases} \frac{\pi}{2} & \text{if } \gamma = 0 \\ \tan^{-1}\left(\frac{\omega}{\gamma}\right) & \text{otherwise.} \end{cases}$$

The same technique can be applied for any pair of filaments. It is interesting to note that although the maximum difference between the mutual inductances calculated using (24), with $\text{dist}_{\text{i,j}}$ as $d_{\text{i,j}}$ (of Fig. 14) used instead of exp(G), is only about 2.4% for the particular example presented later, even this small difference is sufficient to cause major qualitative differences when a large number of mutual inductance terms are calculated in a matrix.

Fortunately, for a rectangular filament, the self-inductance L (or $M_{\text{i,i}}$) can be obtained with high precision using a simple formula which for flyer filaments takes the form [21]

$$L_{\text{f}} = \frac{\mu_0 l}{2\pi}\left(\ln\frac{4l}{2(\Delta yf + \Delta xf)} + \frac{1}{2} + 0.118\frac{2(\Delta yf + \Delta xf)}{l}\right) \quad (28)$$

and a similar expression can be used to calculate the self-inductance of the stator filaments.

To calculate the time rate of change of the mutual inductance, the same technique as in (6) is used: $\partial M_{\text{i,j}}/\partial t = (\partial M_{\text{i,j}}/\partial(\text{dist}_{\text{i,j}}))(\partial(\text{dist}_{\text{i,j}})/\partial t$, with the result of the calculation given later in relation to the flyer dynamics.

D. Flyer 2-D Dynamics

To account for the 2-D deformation of the flyer, it is considered that each of the filamentary columns (along the Oy axis) is capable of moving independently, and *without any friction between neighbours*. In this case, the independent filamentary column dynamics are dictated by the strength of the total force produced electromagnetically and acting on the column, calculated as the summation of all the elementary forces acting on its filaments, all orientated along the Oy-axis. Because of the internal symmetry, the columns in the right-hand side of the flyer (FR) are numbered from the right edge to the left, as in Fig. 15, and the total force acting on the i-th column can be expressed as

$$F_{\text{y}}^{\text{column}}(i) = \sum_{\text{k}=0}^{\text{n}_\text{y}-1} F_{\text{y}}^{\text{filament}}(i + k\, n_{\text{x}}) \quad (29)$$

where $F_{\text{y}}^{\text{filament}}(j)$ is the force acting on the $j = i + kn_{\text{x}}$ filament, which is a part of column i. This force represents the interaction of the current flowing through this filament with each of the magnetic fields produced by all the other filaments, both from the stator as well as from the flyer. Because of the particular shape of the filamentary cross sections (thin plates, as discussed above), the two components of the magnetic field produced by one filament and the resulting interaction forces with the current flowing through any other filament have to be calculated using the integration techniques detailed in the 0-D model, with the result for the force presented in (10a). The complication is that this formula has been obtained for a transmission line made from two thin parallel plates positioned *symmetrically*, i.e., having their centers along the same perpendicular to one of their sides, while for most of the filaments their cross sections are positioned *asymmetrically*. In reference to Fig. 14, for a pair of filaments placed either symmetrically or asymmetrically both situated in the right-hand sides of the

stator and the flyer (FRSR), the accelerating force acting along Oy on the flyer filament is calculated as

$$F_{\mathrm{y}}^{\mathrm{FRSR}}(i,j) = \frac{\mu_0 I_{\mathrm{i}} I_{\mathrm{j}} l}{2\pi\cdot\Delta xs\cdot\Delta xs}\left\{\frac{Y}{2}\ln\left[\frac{\left[\left(\frac{X_1}{Y}\right)^2+1\right]\left[\left(\frac{X_4}{Y}\right)^2+1\right]}{\left[\left(\frac{X_2}{Y}\right)^2+1\right]\left[\left(\frac{X_3}{Y}\right)^2+1\right]}\right]\right. - X_1\tan^{-1}\left(\frac{X_1}{Y}\right)+X_2\tan^{-1}\left(\frac{X_2}{Y}\right) + X_3\tan^{-1}\left(\frac{X_3}{Y}\right) \left. - X_4\tan^{-1}\left(\frac{X_4}{Y}\right)\right\} \quad (30)$$

where $Y = ys(i) - yf(j)$ with $Y \neq 0$ and

$$X1 = xf(j) + \frac{\Delta xf}{2} - xs(i) - \frac{\Delta xs}{2}$$
$$X2 = xf(j) + \frac{\Delta xf}{2} - xs(i) + \frac{\Delta xs}{2}$$
$$X3 = xf(j) - \frac{\Delta xf}{2} - xs(i) - \frac{\Delta xs}{2}$$
$$X4 = xf(j) - \frac{\Delta xf}{2} - xs(i) + \frac{\Delta xs}{2}.$$

The same technique applies for a pair of filaments in the flyer. For $Y = 0$, i.e., when two filaments in the flyer are at the same height, F_{y} is zero.

An analysis of the interaction between filamentary forces shows that:

- Initially, when the flyer is flat, the centers of all flyer columns are at the same height. In this case, the sum of all *internal* vertical forces acting on each column is null. The internal filamentary forces generated between pairs of flyer filaments are along the Oy axis, with the filament placed above being accelerated (the force positive in respect to Oy) while the one below is decelerated (the force is negative). In other words, for a flat and incompressible flyer *the internal vertical forces exactly cancel*, and therefore they do not influence in any way the flyer shape.
- Because of inductive effects, the current distribution in both the stator and in the flyer is clearly nonhomogeneous. This effect influences the flyer dynamics: some columns will move faster than others and therefore an accelerated flyer will never remain flat. Related to this, it is also easy to see that during a shot the sum of all *internal* filamentary forces acting on a column moving ahead is always negative, i.e., the net internal force acts in a direction opposed to the accelerating force produced by the stator filaments. Interestingly, this means that *the internal forces tend to oppose any flyer deformation!*
- Due to magnetic field diffusion in both the stator and in the flyer, the current distribution during a shot spreads more and more inside the material, thus reducing the magnitude of the surface current. As a consequence the accelerating force calculated with a 0-D model, where only surface currents exist, is *always larger* than the total accelerating force calculated with a 2-D model. *The final kinetic energy of the flyer is therefore reduced in a 2-D model in comparison with a 0-D model.*

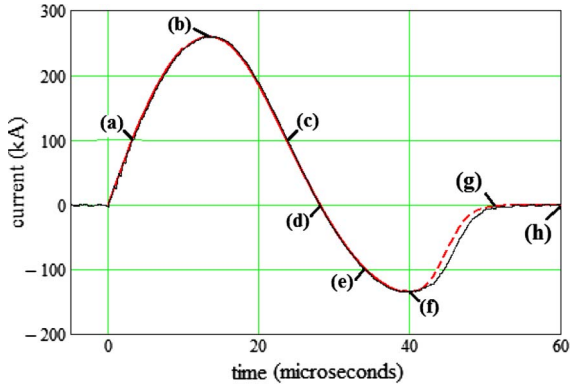

Fig. 16. System current during a shot continuous line: experiment; dotted line: 2D theory. Letters indicate the times for which the current and temperature distributions are shown in Figs. 17 and 18, respectively.

Once the electromagnetically produced forces acting on columns are found, the calculation of the column dynamics is straightforward and the equations of motion are

$$\frac{dv^{\mathrm{column}}(i)}{dt} = \frac{F^{\mathrm{column}}(i)}{m_{\mathrm{column}}} \quad (31)$$
$$\frac{dy^{\mathrm{column}}(i)}{dt} = v^{\mathrm{column}}(i) \quad (32)$$

where $F^{\mathrm{column}}(i)$ is the total force acting on the i-th column similar to (14), and $v^{\mathrm{column}}(i)$ and $y^{\mathrm{column}}(i)$ stand for the i-th column vertical velocity and position, respectively, with initial conditions $v^{\mathrm{column}}(i)|_{t=0}$ and $y^{\mathrm{column}}(i)|_{t=0} = d/2$. The column mass is $m_{\mathrm{column}} = n_{\mathrm{y}}\rho_{\mathrm{flyer}} l\Delta yf\Delta xf$, where ρ_{flyer} is the mass density of the flyer.

The resultant system of differential equations contains $3N + 2(n_{\mathrm{x}}+1)$ equations, corresponding to an equal number of unknowns: N filamentary currents; the charge released in the circuit; the Joule energy deposited into the fuse; N flyer filamentary Joule energies, N stator filamentary Joule energies; n_{x} flyer column velocities and finally n_{x} column positions. The system is firstly solved algebraically for the time rate of change of the unknowns and then integrated using the initial conditions. More information about the implementation of the 2-D filamentary technique can be found in [12].

E. Theoretical Predictions Compared With Experimental Data

The main results obtained using 2D modelling are shown in Figs. 16–21 for the same experimental data as presented in Section II. The flyer and the stator are each represented by a total collection of $2N = 2n_{\mathrm{x}}n_{\mathrm{y}} = 2\times 20\times 10 = 400$ filaments, with 200 independent currents. The total number of differential equations to be integrated in this case is 642. The program is written using MATHCAD 15 and a complete run over 60 μs on a PC operated under Windows 7 with an Intel Core i7 X980 CPU @ 3.33 GHz and with 12 GB RAM takes about a day.

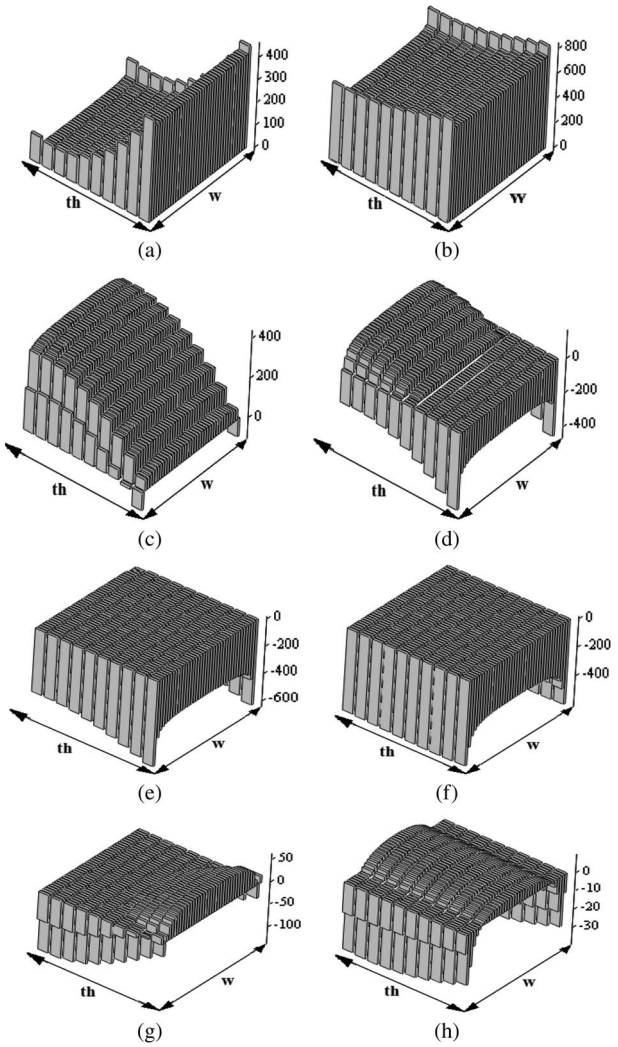

Fig. 17. Current distribution inside the flyer at the various times indicated in Fig. 16 with the vertical scale indicating the filamentary current in Amperes. In reference to Fig. 13, the filamentary currents are calculated only in the right-hand side (FR) and the left-hand side currents are obtained assuming symmetry. The flyer sides are indicated.

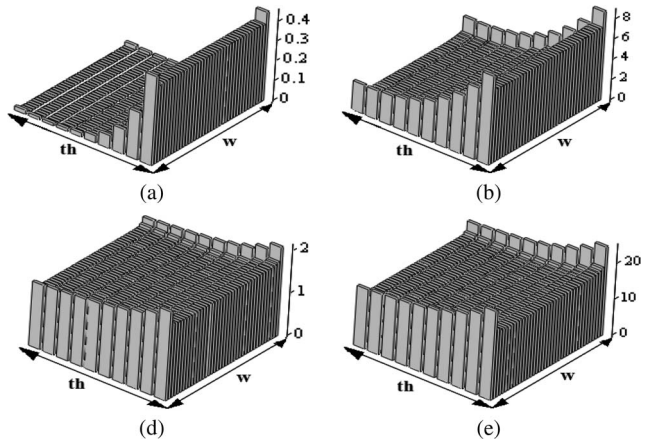

Fig. 18. Temperature *variation* inside the flyer during an experiment the temperature variation is very small and for saving space it is only provided at four of the eight times indicated in Fig. 16.

The results contain considerable useful information, both from the point of view of a designer trying to maintain the flyer surface as flat as possible and also allowing a clear understanding and interpretation of data obtained from various diagnostic tools used in the experiments, such as heterodyne velocimetry technique, ultrahigh speed cameras, or flash X-ray systems. An example of how the model can help in understanding the acceleration phenomena is given below.

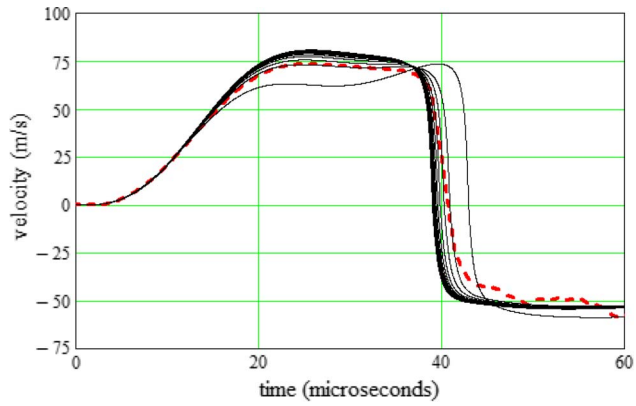

Fig. 19. Time dependence of the flyer velocity. Continuous lines: velocities of the flyer columns calculated using the 2D model. Dotted line: experimental data from heterodyne Velocimetry technique [6].

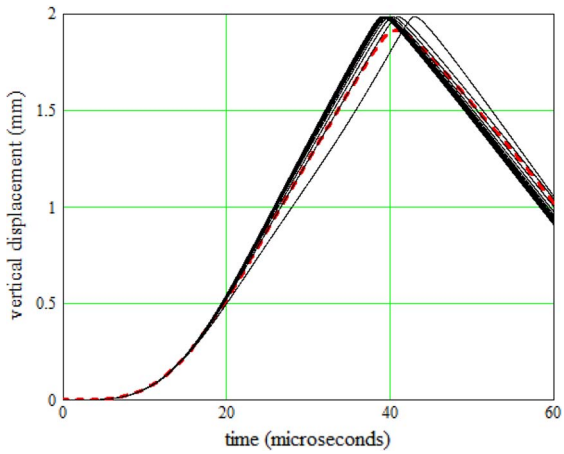

Fig. 20. Flyer dynamics. Continuous lines: vertical displacement of the flyer columns calculated using the 2D model. Dotted line: integrated experimental data from Fig. 7.

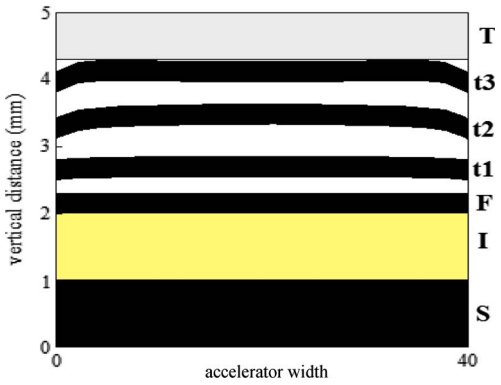

Fig. 21. Flyer shape (cross section in the Oxy plane of Fig. 12) at different moments during the first phase of acceleration, $t1 = 20\ \mu$s, $t2 = 30\ \mu$s, and $t3 = 40\ \mu$s, S-stator, I-insulator, F-flyer (initial position), T-target. The number of flyer columns is indicated along the accelerator width (drawing not to scale).

As presented in Fig. 17, inductive effects concentrate the current distribution towards the flyer edges, and *therefore it could be expected for these to be accelerated ahead of the rest*

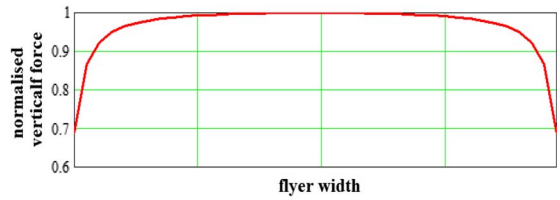

Fig. 22. Normalised force distribution along a static flyer width, for a DC current flowing through the circuit.

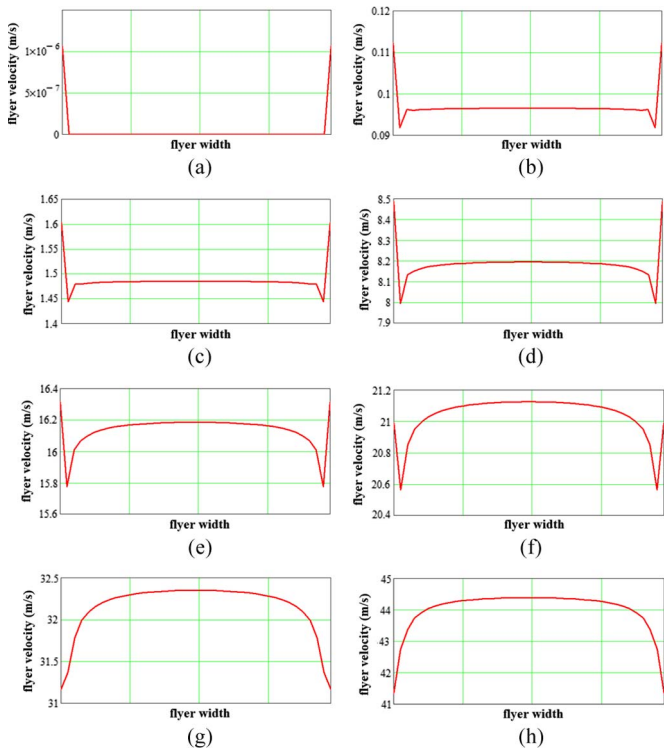

Fig. 23. Velocity distribution along the flyer width at various times during a shot: (a) 1.1 μs; (b) 2 μs; (c) 4 μs; (d) 7 μs; (e) 9 μs; (f) 10 μs; (g) 12 μs; (h) 14 μs.

of the flyer's material. However, the results in Fig. 21 show that during acceleration, the flyer shape does not correspond to the shape predicted by these simple arguments, i.e., *the flyer edges lag behind!*

To understand this intriguing phenomenon, consider the forces acting on flyer columns in DC conditions (i.e., when the current distribution is homogeneous), and Fig. 22 shows the result for this particular arrangement. The force acting on the column positioned at the flyer's edge is 1.45 times less powerful than that acting on the column situated in the flyer's center. This means that, when applying transient currents, these two forces will be equal only for a certain current distribution. A very *rough estimation* shows that, by neglecting the flyer thickness, the current density at edge is required to be $\sqrt{1.45} \approx 1.2$ times the current density in the center. For the particular arrangement considered, this will only happen but for an extremely short period of time.

The details of the first 14 μs of a shot are very interesting (Fig. 23) and show the complexity of the first moments of the flyer acceleration phenomenon. In the first microsecond after the current begins to flow the flyer is stationary, i.e., the gravitational force is larger than the force generated electromagnetically. The first movement of the flyer edges is predicted at 1.1 μs [Fig. 23(a)] and at 2 μs the velocity is already over 0.11 m/s [Fig. 23(b)]. The flyer acceleration continues with edges ahead [Fig. 23(c) and (d)], but slowly, these lose speed in respect to the center [Fig. 23(e) and (f)], and finally the velocity distribution radically changes [Fig. 23(g) and (h)]. After 14 μs, the relative velocity distribution and the flyer's shape remain more or less the same (even though the flyer accelerates) until the flyer approaches the target.

IV. Conclusions and the Way Ahead

Two numerical models have been developed jointly by Loughborough University and AWE, Aldermaston, for predicting the characteristics of a flat parallel-plate electromagnetic accelerator.

The first, a 0-D model, has the advantage of being extremely fast and is ideally suited for use in the parametric studies required in the design of new arrangements.

The second, a very detailed 2-D model, provides more detailed information and uses original calculation techniques.

Future work may include the development of a complex multiphysics 3-D finite-element analysis model. This code will account for elastoplastic properties and the generation of shock waves, the variation of electrical conductivity with pressure, and other related phenomena. This final stage of modelling may also include the new element of the complex physics associated with the flyer-target interaction.

References

[1] R. W. Lemke, M. D. Knudson, and J.-P. Davis, "Magnetically driven hyper-velocity launch capability at the Sandia Z accelerator," *Int. J. Impact Eng.*, vol. 38, no. 6, pp. 480–485, Jun. 2011.

[2] T. Ao, J. R. Asay, S. Chantrenne, M. R. Baer, and C. A. Hall, "A compact strip-line pulsed power generator for isentropic compression experiments," *Rev. Sci. Instrum.*, vol. 79, no. 1, p. 013903, Jan. 2008.

[3] G. Wang, C. Sun, F. Tan, J. Zhao, N. Zhang, C. Liu, J. Mo, G. Wang, and X. Wang, "The compact capacitor bank CQ-1.5 employed in magnetically driven isentropic compression and high velocity flyer plate experiments," *Rev. Sci. Instrum.*, vol. 79, no. 5, p. 053904, May 2008.

[4] D. B. Seidel, W. L. Langston, R. S. Coats, M. D. Knudson, R. W. Lemke, J.-P. Davis, and T. D. Pointon, "An optimization study of stripline loads for isentropic compression experiments," in *Proc. 17th IEEE Int. Pulsed Power Conf.*, Jun. 28–Jul. 2 2009, pp. 1165–1170.

[5] A. Lefrançois, P.-Y. Chanal, G. Le Blanc, J. Petit, G. Avrillaud, and M. Delchambre, "High-velocity flyer-plate developments on two high-pulsed-power generators based on a strip-line design (GEPI and CEPAGE)," *IEEE Trans. Plasma Sci.*, vol. 39, no. 1, pp. 288–293, Jan. 2011.

[6] K. Omar, N. Graneau, M. Sinclair, B. M. Novac, and I. R. Smith, "Foil flyer electro-magnetic accelerator—Initial results from a new AWE pulsed power generator," in *Proc. 18th IEEE Int. Pulsed Power Conf.*, Chicago, IL, Jun. 19–23, 2011.

[7] H. Knoepfel, *Pulsed High Magnetic Fields*. London, U.K.: North-Holland Publ., 1970.

[8] C. S. Walker, *Capacitance, Inductance and Crosstalk Analysis*. Boston, MA: Artech House, 1990.

[9] R. Bealing and P. G. Carpenter, "Efficient magnetic flier plate propulsion," *J. Phys D, Appl. Phys.*, vol. 9, no. 2, pp. 151–159, Feb. 1976.

[10] R. Bealing and P. G. Carpenter, "A compact 2 MJ capacitor bank," AWRE Rep. 02/76.

[11] R. A. Benham, "Preliminary experiments using light-initiated high explosives for driving thin flyer plates," Sandia Nat. Lab., Albuquerque, NM, Technical Report, SAND79-1847, 1979.

[12] C. Mielke and B. M. Novac, "Experimental and numerical studies of Megagauss magnetic field generation at LANL-NHMFL," *IEEE Trans. Plasma Sci.*, vol. 38, no. 8, pp. 1739–1749, Aug. 2010.
[13] B. M. Novac, I. R. Smith, and M. C. Enache, "Accurate modeling of the proximity effect in helical flux-compression generators," *IEEE Trans. Plasma Sci.*, vol. 28, no. 5, pp. 1353–1355, Oct. 2000.
[14] B. M. Novac, I. R. Smith, M. C. Enache, and H. R. Stewardson, "Simple 2D model for helical flux-compression generators," *Laser Particle Beams*, vol. 15, no. 3, pp. 379–95, 1997.
[15] K. Gregory, I. R. Smith, V. V. Vadher, and M. J. Edwards, "Experimental validation of a capacitor discharge induction launcher model," *IEEE. Trans. Magn.*, vol. 31, no. 1, pp. 599–603, Jan. 1995.
[16] B. M. Novac, I. R. Smith, M. C. Enache, and P. Senior, "Studies of a very high efficiency electromagnetic launcher," *J. Phys. D, Appl. Phys.*, vol. 35, no. 12, pp. 1447–1457, Jun. 2002.
[17] B. M. Novac, I. R. Smith, P. E. Jarvis, and C. J. Abbott, "Accelerating conductors by electromagnetic action through metallic shields," *IEEE. Trans. Magn.*, vol. 39, no. 1, pp. 305–309, Jan. 2003.
[18] B. M. Novac, I. R. Smith, and M. Hubbard, "2D modeling of electromagnetic flux-compression in θ-pinch geometry," *IEEE Trans. Plasma Sci.*, vol. 32, no. 5, pp. 1896–1901, Oct. 2004.
[19] J. Luo, B. M. Novac, I. R. Smith, and J. Brown, "Fast and accurate two-dimensional modelling of high-current, high-voltage air-cored transformers," *J. Phys. D, Appl. Phys.*, vol. 38, no. 6, pp. 955–963, Mar. 2005.
[20] A. Y. Wu and K. S. Sun, "Formulation and implementation of the current filament method for analysis of current diffusion and heating in conductors in railguns and homopolar generators," *IEEE. Trans. Magn.*, vol. 25, no. 1, pp. 610–615, Jan. 1989.
[21] F. W. Grover, *Inductance Calculations. Working Formulas and Tables*. New York: Dover, 1946.
[22] E. B. Rosa, "On the geometrical mean distances of rectangular areas and the calculation of self-inductance," *Bull. Bur. Standards*, vol. 3, pp. 5–41, Apr. 1907.
[23] "ALEGRA: An arbitrary Lagrangian-Eulerian multimaterial, multiphysics code," presented at the 46th AIAA Aerospace Science Meeting Exhibit, Reno, NV, 2008, AAIAA 2008-12351e39.
[24] D. G. Tasker, "Megabar Isentropic Compression Experiments (ICE) using High Explosive Pulsed Power (HEPP)," Ph.D. dissertation, Loughborough Univ., Leicestershire, U.K., 2006.
[25] D. G. Tasker, "Megabar Isentropic Compression Experiments (ICE) using High Explosive Pulsed Power (HEPP)," Los Alamos Nat. Univ., Los Alamos, NM, LANL Report LA-UR-06-8522, 2006.

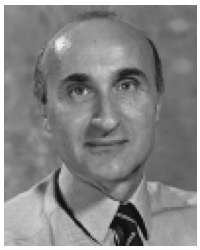

Bucur M. Novac (M'07–SM'08) received the M.Sc. and Ph.D. degrees from the University of Bucharest. He was a full-time employee at the Institute of Atomic Physics from 1977, working in the Plasma Physics Laboratory and serving as Head of the laboratory from 1993 to 1998.

He joined the Loughborough University, U.K., in 1998, and is currently Professor of pulsed power.

His research interests include compact high-power systems, explosively and electromagnetically driven magnetic flux compression generators, and their applications, electromagnetic launchers, ultrafast magneto and electro-optic sensors, and 2-D modeling of pulsed-power systems.

Dr. Novac is a Fellow of The Institution of Engineering and Technology.

Kaashif Omar was born in Leicester in 1985. He received the MPhys degree in Physics with Astrophysics from the University of Leicester, in 2007. He joined Atomic Weapons Establishment, Aldermaston as a graduate at the end of 2007 and is now working as an Experimental Physicist developing high current pulsed power machines for dynamic materials property research. He is also working towards a part time PhD at Loughborough University.

Neal Graneau received the BSc degree in Physics from King's College, London University, in 1986, and the MSc and D.Phil degrees in Plasma Physics from the University of Oxford, in 1987 and 1992, respectively. He is currently a Senior Scientist at Atomic Weapons Establishment, leading the development of high current pulsed power machines for dynamic material properties research. His research interests span from experiments in fundamental electromagnetism and their implication in matter interaction theories to renewable energy devices exploiting the electrical manipulation of liquids. He has authored and co-authored three books, two chapters for edited volumes, 25 refereed journal articles, and 15 conference papers.

Ivor R. Smith (M'09–SM'11) received the B.Sc. and Ph.D. degrees from the University of Bristol, U.K., after completing a student apprenticeship at the Witton Works of the General Electric Company.

He then became a Lecturer in electrical engineering at the University of Birmingham, Birmingham, U.K., subsequently being promoted to Lecturer and Reader and being awarded the degree of D.Sc. for his continued research contribution. He then moved to Loughborough University to become Professor of Electrical Power Engineering, and serving as Head of Department, Dean of Engineering, and Pro-Vice Chancellor. For some 25 years, he has been active in research in many aspects of the production, conditioning, and utilization of large pulses of electrical energy, and his work has brought in very substantial funding from a wide range of sponsors.

Dr. Smith is a Chartered Engineer, a Fellow of The Institution of Engineering and Technology, and of the Royal Academy of Engineering.

Mark Sinclair (M'03) received the B.Sc. degree from the Victoria University of Manchester, U.K., in 1990, and then went to St. Andrews and Strathclyde Universities in Scotland to receive the M.Sc. in laser engineering and pulsed power technology. In 1992, he joined the Pulsed Power Group at Atomic Weapons Establishment (AWE). Initially, he worked on the E Minor machine moving on to Mogul E which was optimized for radiography of dense objects. Currently, he is the technical lead for pulsed power at AWE overseeing a number of programmes to develop fundamental knowledge and skills, to develop new X-ray sources, and to use pulsed power for hydrodynamic simulation.